An Efficient Direct Time-of-Flight (dToF) LiDAR System Based on High Resolution SPAD Array

Tze Ching Fung*, Chunji Wang, Hongyu Wang, Alfonso Cesar Barredo Albason, Radwanul Hasan Siddique and Yibing M. Wang

Meta Vision Lab, Samsung Semiconductor Inc., Pasadena CA, USA
*Email: richard.fung@samsung.com

***Abstract*—We proposed a LiDAR system for mobile application that is power efficient and tolerates high ambient. The system has 940nm scanning laser sources and a 192×144 single-photon avalanche diode (SPAD) array with on-chip time correlated histogramming. The adaptive single-pass histogramming architecture saves power by staying at coarse resolution mode when returned laser pulses are weak. New signal processing method allows a depth resolution beyond coarse bin size. The system is able to measure depth images at 30 fps, with up to 10 meters range, 1% range error, and only consumes 12 mW optical power.**

Keywords—LiDAR, SPAD, dTOF, adaptive, single-pass, histogram

I. INTRODUCTION

Depth sensing has become a salient feature in applications that involve environmental interactions, such as augmented reality (AR), self-driving vehicles, and security surveillance. Among common ranging technologies like radar and ultrasonic, Light Detection and Ranging (LiDAR) sensors have advantages of long range, high range resolution, and high spatial resolution. LiDAR resolves depth via measuring the time of flight (ToF) of light between the sensor and the detected object. According to different measurement principles, it is often categorized either as direct time of flight (dToF) [1] or indirect time of flight (iToF) [2] types. dToF is of particular interest due to its immunity to multi-path echo and the ease of augmenting it with existing vision systems to form a 3D image solution [3].

A dToF LiDAR sensor needs to reject the background light (aka ambient) from the transmitted light by repetitive measurement. To detect returned laser photons from all photons, a histogram is typically used to bin the photon timestamps, and the peak of the histogram usually indicates returned laser photons. It can be quite challenging to design a system that strikes the right balance between power efficiency, ambient tolerance, range, and range resolution. Increasing light source intensity or reducing histogram bin size often warrant better performance; but the increase in power consumption and memory may negate the benefit. A two-pass solution has been proposed [4] to mitigate this issue. It first uses a coarse histogram to estimate depth in coarse resolution, then build a new fine histogram around the estimated coarse depth, so that a fine resolution depth is obtained. Nonetheless, the signals in the first pass are discarded before the second pass, making no contribution to improve range resolution. The impact of signal loss (or waste) is especially pronounce at long range measurement where returned photons are usually fewer and therefore more valuable.

In this paper, we present a design of a LiDAR system using 192×144 SPAD array. The system features an adaptive single pass histogramming architecture that allows the histogram to adaptively switch from coarse mode to fine mode depending on returned laser signals strength. Together with novel signal processing, the system is capable to detect low albedo (10%) objects with high resolution at 10 meters under full sun outdoor, at 30 frames per second (fps), at low power consumption.

II. SYSTEM ARCHITECTURE

The system architecture is illustrated in Figure 1. We adopted scanning LiDAR scheme to take advantage of its higher signal-to-noise ratio (SNR) than non-scanning ones (e.g. Flash LiDAR) [5]. Different types of laser beam scanners have been investigated for LiDAR application; among those, solid-state scanners are often preferred due to no moving parts, fast response time, potential for a compact design, and low cost [6]. Especially recent advancement in combining laser diode array with diffractive optics element (DOE)

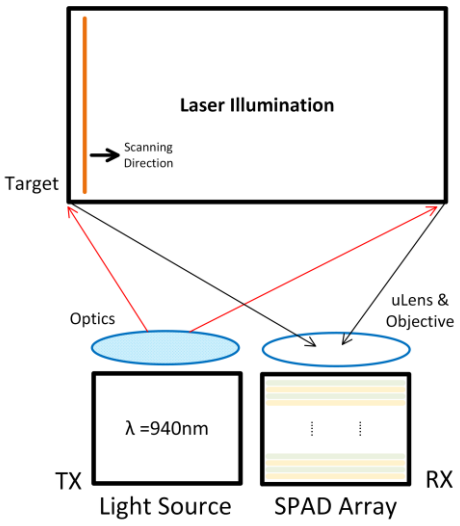

Figure 1. Proposed LiDAR system in this work including a 940nm infrared light source as transmitter (TX) and an addressable SPAD array as receiver (RX).

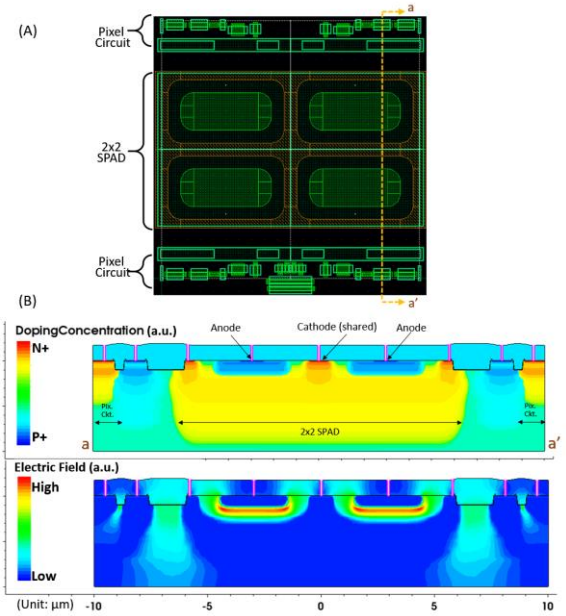

Figure 2. (A) The 20μm pixel layout, and (B) cross-sectional view in doping concentration and electrical filed distribution by TCAD simulation.

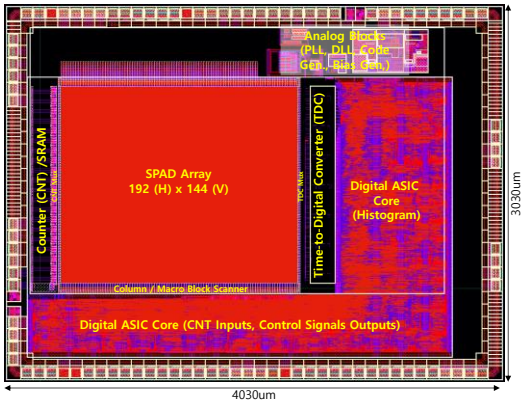

Figure 3. Layout of 90nm BSI SPAD sensor chip (RX).

makes them very attractive in LiDAR systems for consumer products [7].

The TX consists of a laser scanner with optical elements illuminating the field with line patterns at an infrared wavelength of 940 nm. Due to the optical disparity between the laser patterns and the light signals reflected back from the target, the interrogation pattern spacing cannot be uniform throughout. We designed the SPAD array in the receiver (RX) with a flexible addressing scheme to avoid missing reflected light signals, which is achieved by dividing the SPAD array into different regions, such that the scanning and addressing patterns within each regions can be set independently. As a result, the RX scanning patterns can be tuned to match perfectly with the changing reflected light locations to guarantee the capture of returned signal photons.

As will be described in detail below, the RX chip has also counter (CNT) and time-to-digital converter (TDC) circuits placed on both sides of the array

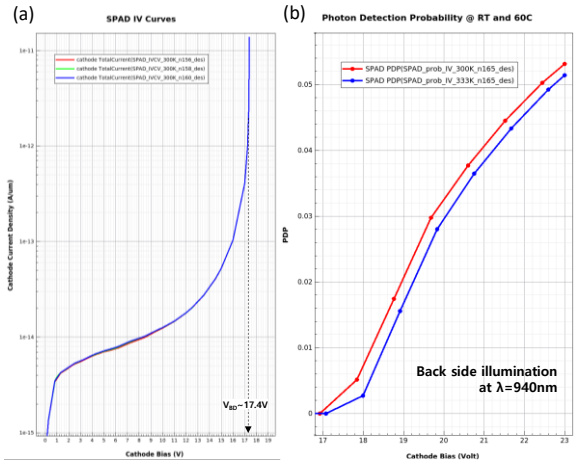

Figure 4. TCAD simulation of (a) SPAD reverse bias I-V curve and (b) PDP as a function of cathode bias.

allowing SPAD voltage pulses to be processed immediately after photons being detected. In addition, with on-chip ASIC supporting full histogram building and readout, the proposed LiDAR system is capable of real-time depth sensing at 30 fps.

III. SPAD Sensor Chip and Operation

We designed the RX with all the essential blocks to conduct the dTOF operation fully on-chip. Figure 5 illustrates the SPAD sensor chip architecture, signal paths, and the 2 × 2 SPAD pixel circuit. A SPAD typically operates in avalanche breakdown region with a reverse bias slightly exceeding its breakdown voltage (i.e. $V_{bias} = V_{bd} + V_{ex}$) with V_{ex} being the excess voltage). This means SPAD has very high signal gain and can detect single-photon events. To reset an excited SPAD back to its stand-by state, a quenching transistor is connected at the anode (aka passive quenching) [8]. This makes a compact SPAD design difficult to achieve. Recently virtual guard ring based SPAD designs have shown to be promising in achieving small pitch [9]. We built upon a similar concept, and further improved the fill factor (to 19.6%) by sharing one common cathode and output circuit with four (2×2) neighboring SPADs in a 20 μm pixel (refer to Figure 2). The SPAD has a pitch of 10 μm, and we designed the breakdown voltage (V_{bd}) at 17.4V. The four SPAD output channels are coupled through an OR gate as a unified pixel output to save circuit area and improve fill factor. Signal processing of the combined pulses will be discussed in detail in Section IV. The SPAD sensor chip is fabricated by Samsung's custom 90 nm back-side illumination (BSI) image sensor process. TCAD simulations confirmed the present design can achieve photo detection probability (PDP) of 3% at 940nm with an excess voltage (Vex) of 2.6V (Fig.4). By optimizing device structure, incorporating metalens to improve effective fill factor, and nanostructured thin-film to enhance light absorption, we estimate a greater than 3-folds improvement with epi-thickness of 3um, or photo detection efficiency (PDE) above 10% in final designs.

As shown in Figure 6, the dTOF operational sequence can be separated into two parts: locating

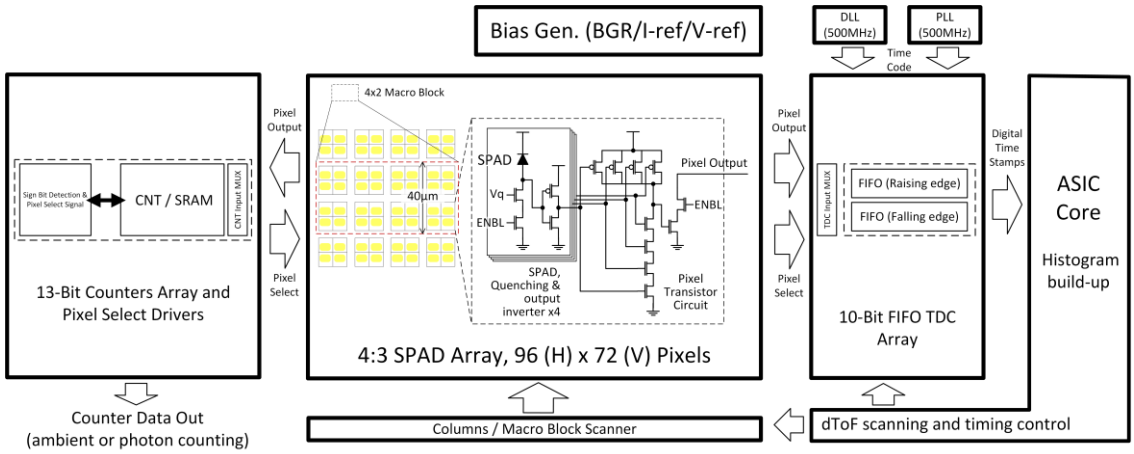

Figure 5. Sensor chip (RX) architecture. The SPAD array has a total of 96×72 (2×2 SPAD) pixels and the inset illustrates the 2×2 SPAD pixel circuit. The 13-bit counters (CNT) and dual 10-bit time-to-digital converters (TDC) are located on the left and right side of array, respectively.

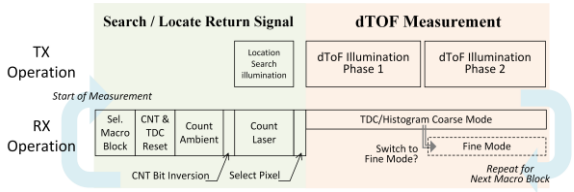

Figure 6. dToF operational sequence of one line scan. The sequence repeated itself until the TX scans through the entire scene.

reflective laser signals followed by repetitive dTOF measurement cycles.

At the beginning of return signal search, new groups of pixels are enabled by signals from column/ macro block scanner (ref. Figure 5, located at the bottom of array). As can be seen in Figure 5, eight (4×2) neighboring pixels are addressed together as a macro block, so the returned laser photons can be captured regardless of disparity. Once the macro block is selected, the 13-bits CNT array first counts the ambient photons for all pixels within the block. CNT bit inversion (2's compliment) is then performed followed by another round of photon counting under laser illumination (labeled "location search" in Figure 6). Exact return laser signal location can then be determined by detecting which CNT (hence pixel) first has its sign bit flipped to positive. Such operation allows us to design the array with just a simple upward CNT instead of a more complicated bidirectional (up/down) one. At the end of this phase, CNT array sends out the pixel select signals which drive the TDC input MUX. Therefore, only the pixel that received the highest amount of photons is selected for dToF measurement.

During the dTOF measurement phase, digital pulse trains from SPAD array are processed by high precision TDC capable of resolving time stamps down to 250 ps. The total number N of laser pulses to be projected is determined by the maximum range to be measured. Midway through the measurement, the ASIC logic analyzes histogram from the first M cycles and determines if it should switch to the fine bin mode. This dTOF operation is repeated until it scans through the entire SPAD array.

IV. Signal Processing

Since the laser pulse is quite wide (e.g. w = 4 ns, about 0.6 meter in distance), edge triggering is required to achieve the desired resolution (1% of range). We designed the signal processing pipeline (i.e. TDC) to accurately measure the time stamps of rising and falling edges of returned pulses. The signal processing pipeline consists of pulse collection recovery, histogramming, and post-processing.

When two or more SPADs give pulses simultaneously, they merge into a single pulse on the readout channel (we call this process "pulse collision" or "event collision"), leading to signal loss. Pulse collision happens more frequently if a single SPAD pulse is longer. When pulses collide, only the first pulse leading edge and the last pulse trailing edge survive; other edges are lost.

This is similar to photon pile-up [10] in that later photons get masked by earlier photons. Pulse collision compounds with pile-up, distorts the photon counts and introduces depth measurement error. To alleviate this signal loss, we developed pulse collision recovery algorithm (Figure 7A) to recover most of the lost signal. To do this, TDC records both the leading and trailing edges timestamps (t_1 and t_2) of a pulse. If $t_2 - t_1$ is greater than the single pulse width (w_S) in a single SPAD channel (obtained via calibration), then we can recover one more event timestamp at $t_2 - w_S$. We show an example in Figure 7A, in which three SPADs detect in total 6 photons, but the merged channel only shows 3 pulses. The collision recovery algorithm recovers 2 out of 3 lost photon-detection events. Even though not all photons are recovered, simulation shows in Figure 7B that this recovery algorithm leads to result approaching to the case without collision at all. This is because the probability of n pulses colliding decreases dramatically with n, so for the majority of collision cases, those of two pulses colliding, are fully recovered.

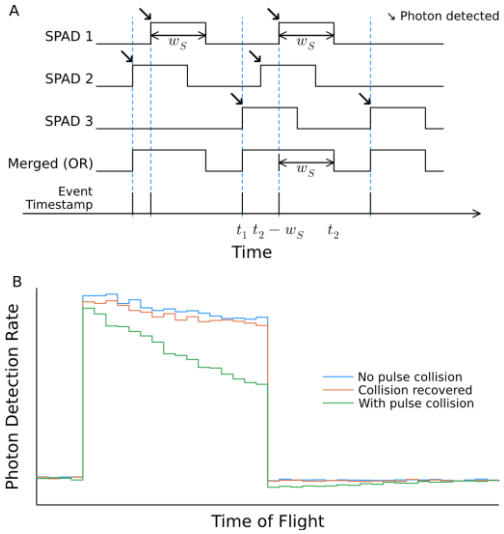

Figure 7. (A) Collision recovery algorithm example showing three SPAD channels merging into one channel. (B) Simulated histogram with pulse collision and its recovery algorithm. Target albedo is 0.5 at 7 meters, under half of outdoor full-sun ambient.

To obtain precise TOF from the fine histogram, it is necessary to apply a digital filter to enhance the peak. To avoid pile-up induced issues, we developed a conditional FIR filter for accurate peak enhancement. Figure 8D illustrates an example by simulation. The resolved TOF matches well to the peak location of the filtered histogram.

V. Performance Estimation and Conclusion

We numerically simulated the system with Monte Carlo method to estimate system measurement error. As shown in Figure 9, the error keeps within 1% of range, except at extremely close range below 1.5 m, where the error cannot be reduced beyond fine bin resolution (250 ps, equivalently 3.75 cm). Table 1 gives a summary of the system specs. In conclusion, we reported a complete LiDAR system design including TX, RX, on-chip histogramming and data processing. The TX is based on laser scanner illuminating at 940nm. The RX has a SPAD array with a flexible addressing scheme for disparity-agnostic return signal

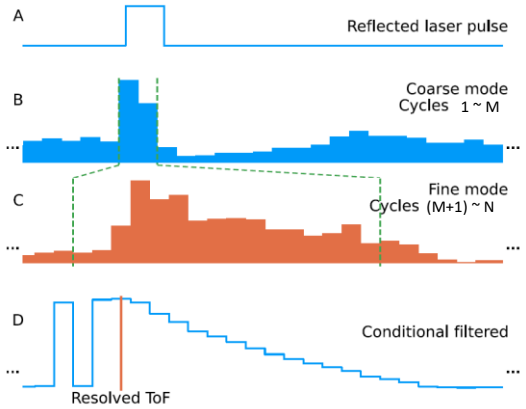

Figure 8. Adaptive single pass histogram, switching from coarse to fine mode in the middle of the N cycles. (D) shows a conditional FIR filter.

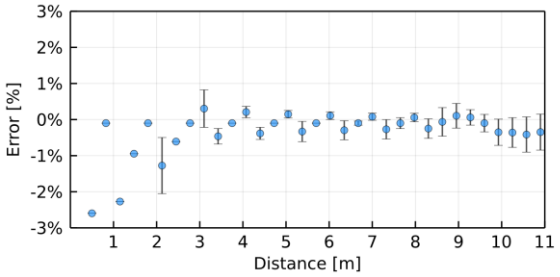

Figure 9. Simulated measurement error. Each data point and represents statistic of 100 repeated measures. Target albedo is randomly sampled from 0.1 to 0.8; ambient level is randomly sampled from 0%~100% full sun ambient.

locating. On-chip adaptive single-pass histogram shows superior performance compared to time-gated solutions [4] under limited optical power budget. The system is capable of capturing depth images at 30 fps at 12 mW optical power. The system has a range of up to 10 meters, and depth error is kept within 1%. The system is well-balanced between energy efficiency, range, range resolution and ambient tolerance, making it suitable for mobile ranging application.

TABLE I. System Characteristic (Simulation)

System Specification	***Value***
Avergae Opt. Power	12mW
Maximum Range	10 meters
Range Precision	< 1% × range
Frame Rate	30 fps
TDC Resolution	250 psec

References

[1] Gongbo Chen, Christian Wiede, and Rainer Kokozinski, “Data Processing Approaches on SPAD-Based d-TOF LiDAR Systems: A Review,” IEEE Sensors Journal, 21(5):5656–5667, Mar.

[2] Cyrus Bamji, John Godbaz, Minseok Oh, Swati Mehta, Andrew Payne, Sergio Ortiz, Satyadev Nagaraja, Travis Perry, and Barry Thompson, ”A review of indirect time-of-flight technologies,” IEEE Trans. Electron Devices, 2022.–73.

[3] I. Gyongy, N. A. W. Dutton and R. K. Henderson, "Direct Time-of-Flight Single-Photon Imaging," in IEEE TED, vol. 69, no. 6, pp. 2794-2805, June 2022

[4] AK Sharma, A Laflaquiere, GA Agranov, G Rosenblum, and S Mandai, “Spad array with gated histogram construction,” US Patent 20170052065 A, 1, 2017.

[5] Dingkang Wang, Connor Watkins, and Huikai Xie, “Mems mirrors for lidar: A review,” Micromachines, 11(5), 2020.

[6] Thinal Raj, Fazida Hanim Hashim, Aqilah Baseri Huddin, Mohd Faisal Ibrahim, and Aini Hussain, “A survey on lidar scanning mechanisms,” Electronics, 9(5), 2020.

[7] Yulong An, Yanmei Zhang, Haichao Guo, and Jing Wan, “ Compressive sensing-based threedimensional laser imaging with dual illumination,” IEEE Access, 7:25708–25717, 2019.

[8] Andrea Gallivanoni, Ivan Rech, and Massimo Ghioni,” Progress in quenching circuits for single photon avalanche diodes,” IEEE Trans. on Nuclear Science, 57(6):3815–3826, 2010.

[9] Tomer Leitner et al., “Measurements and simulations of low dark count rate single photon avalanche diode device in a low voltage 180-nm cmos image sensor technology, “IEEE Trans. on Electron Devices, 60(6):1982–1988, 2013.

[10] P B Coates, “The correction for photon ‘pile-up’ in the measurement of radiative lifetimes,” Journal of Physics E: Scientific Instruments, 1(8):878–879, Aug. 1968